Collision-energy Dependence of Deuteron Cumulants and Proton-deuteron Correlations in Au+Au collisions at RHIC

The STAR Collaboration [a,]

[a] *Relativistic Heavy-Ion Collider, Brookhaven National Laboratory, NY, USA*

arXiv:2304.10993v1 [nucl-ex] 21 Apr 2023

Abstract

We report the first measurements of cumulants, up to 4^{th} order, of deuteron number distributions and proton-deuteron correlations in Au+Au collisions recorded by the STAR experiment in phase-I of Beam Energy Scan (BES-I) program at the Relativistic Heavy Ion Collider (RHIC). Deuteron cumulants, their ratios, and proton-deuteron mixed cumulants are presented for different collision centralities covering a range of center of mass energy per nucleon pair $\sqrt{s_{\rm NN}}$ = 7.7 to 200 GeV. It is found that the cumulant ratios at lower collision energies favor a canonical ensemble over a grand canonical ensemble in thermal models. An anti-correlation between proton and deuteron multiplicity is observed across all collision energies and centralities, consistent with the expectation from global baryon number conservation. The UrQMD model coupled with a phase-space coalescence mechanism qualitatively reproduces the collision-energy dependence of cumulant ratios and proton-deuteron correlations.

Keywords: Heavy-ion collisions, Deuteron production, Coalescence, Thermal model, Higher moments, Critical point

1. Introduction

One of the major goals of heavy-ion collision experiments is to study the phases of strongly interacting nuclear matter versus temperature and pressure. Experimental results have demonstrated the existence of a deconfined state of quarks and gluons [1–6]. The mean yields of hadrons produced in central heavy-ion collisions can be described by thermal models with a suitable choice of chemical freeze-out parameters such as temperature (T) and baryon chemical potential (μ_B). The typical values of T vary from around 140 MeV at collision energy ($\sqrt{s_{\rm NN}}$) of 7.7 GeV to 160 MeV at the energy of 5.02 TeV [7–9]. However, deuterons, tritons, and other light nuclei, which have binding energies of the order of a few MeV, are also produced in heavy-ion collisions [10–12]. Interestingly, the yields of light nuclei can also be explained with temperatures similar to those extracted using hadronic yields [9, 13, 14]. The natural question that arises then is: how are light nuclei produced in a medium that freezes out at the temperature of the order of 100 MeV?

The production mechanism of light nuclei is commonly studied in two approaches: the *thermal model* and the *coalescence model*. The thermal model treats light nuclei as any other hadrons and their masses and quantum numbers are inputs to the model. These model calculations show good agreement with experimental data on transverse momentum ($p_{\rm T}$) integrated mid-rapidity yields of deuterons and deuteron to proton yield ratios in central heavy-ion collisions [9, 10]. In the coalescence model, light nuclei are formed by coalescing protons and neutrons with a finite probability determined by their closeness to each other in the phase-space [15, 16]. One of the signatures of the coalescence mechanism is that the elliptic flow of light nuclei should show constituent nucleon number scaling [17], and such a scaling property has been observed in the STAR experiment [18]. Both the thermal and coalescence models have been fairly successful in explaining the set of experimental data. However, the production mechanism of light nuclei still needs to be understood in detail [13, 19–22]. It is not necessarily true that deuteron production has to happen only via one of the above-mentioned mechanisms. Both mechanisms might be at work in heavy-ion collisions [16].

Furthermore, higher order cumulants of particle multiplicity distributions are known to probe finer details of the thermodynamics of the system created [23–28]. Recent studies suggest that cumulants of event-by-event deuteron number distribution might have different signatures in thermal and coalescence approaches and can shed light on their production mechanism [29]. Calculations using a simplified coalescence model predict the rise of cumulant ratios towards lower collision energies in contrast to the predictions from the thermal model using Grand Canonical Ensemble (GCE) and the Poisson baseline, both of which are equal to 1 across collision energies [29].

In addition to probing the production mechanism, higher moments of deuteron number fluctuation can potentially be sensitive to signals of the QCD critical point, and first-order phase transition. Even though deuteron has a binding energy of only 2.2 MeV, its production is predicted to be affected by the enhancement of pre-clustering of nucleons at the chemical freeze-out due to modifications in the nucleon-nucleon interaction near a phase transition [30, 31]. Also, a certain combination of the proton, deuteron, and triton yields is constructed to probe neutron density fluctuations at the kinetic freeze-out [32] and has been measured by the STAR experiment. These results show an excess over the coalescence baseline in central collisions at $\sqrt{s_{\rm NN}}$ = 19.6 and 27 GeV [33]. Further, as deuterons carry two

baryons, their fluctuation may add to the understanding of the baryon number fluctuations in heavy-ion collisions.

In this paper, we report the first measurements of the cumulants of the deuteron multiplicity distribution and the proton-deuteron number correlation from Au+Au collisions recorded by the STAR detector [34] at RHIC from the years 2010 to 2017. The data are presented for Au+Au collisions at $\sqrt{s_{\rm NN}}$ = 7.7, 11.5, 14.5, 19.6, 27, 39, 54.4, 62.4, and 200 GeV corresponding to a wide range of baryon chemical potential from 420 to 20 MeV [7, 35]. The results are compared to thermal model calculations for Grand Canonical and Canonical Ensembles (GCE and CE) [36], the Ultrarelativistic Quantum Molecular Dynamics (UrQMD) model [37, 38] combined with a phase-space coalescence mechanism [39], and a simplified coalescence model [29].

2. Observables

Distributions can be characterized by their cumulants of various order. A general expression to find any order cumulants of a distribution can be found in [44]. The cumulants (C_n) up to order $n = 4$ are defined below. We use N to represent the number of deuterons in one event and $\langle N\rangle$ for the average value over the entire event ensemble. Then the deviation of N from its event average is given by $\delta N = N - \langle N\rangle$.

$$C_1 = \langle N\rangle \quad (1)$$

$$C_2 = \langle(\delta N)^2\rangle \quad (2)$$

$$C_3 = \langle(\delta N)^3\rangle \quad (3)$$

$$C_4 = \langle(\delta N)^4\rangle - 3\langle(\delta N)^2\rangle^2 \quad (4)$$

The moments can be expressed in terms of the cumulants:

$$M = C_1\,,\quad \sigma^2 = C_2\,,\quad S = \frac{C_3}{C_2^{3/2}}\,,\quad \kappa = \frac{C_4}{C_2^2}\,, \quad (5)$$

where M is the mean, σ is the standard deviation, S is the skewness and κ is the kurtosis.

To eliminate the system volume dependence of cumulants, their ratios are usually constructed as follows [40]:

$$\frac{\sigma^2}{M} = \frac{C_2}{C_1}\,,\quad S\sigma = \frac{C_3}{C_2}\,,\quad \kappa\sigma^2 = \frac{C_4}{C_2}\,. \quad (6)$$

These ratios can be connected to the ratios of number susceptibilities calculated in thermal models [24] as $C_2/C_1 = \chi_2/\chi_1$, $C_3/C_2 = \chi_3/\chi_2$, and $C_4/C_2 = \chi_4/\chi_2$. The n-th order number susceptibility is $\chi_n = d^n[P/T^4]/d(\mu/T)^n$, where P, T, and μ are the equilibrium pressure, temperature, and chemical potential, respectively.

If the particle multiplicity follows the Poisson distribution, cumulants of all orders are equal and therefore their ratios are unity. Poisson expectations are used as the statistical baselines for the measured cumulant ratios.

The Pearson correlation coefficient measures the linear correlation between two variables. The correlation coefficient between proton and deuteron numbers can be defined as follows:

$$\frac{C^{(1,1)}_{(p,d)}}{\sigma_p\sigma_d} = \frac{\langle(\delta N_p\delta N_d)\rangle}{\sigma_p\sigma_d} = \frac{\langle N_pN_d\rangle - \langle N_p\rangle\langle N_d\rangle}{\sigma_p\sigma_d}\,, \quad (7)$$

where N_p and N_d are proton and deuteron numbers, respectively. The correlation coefficient ranges from -1 to 1. A positive sign of the coefficient implies that two variables are correlated while a negative sign implies an anti-correlation. A zero value of the coefficient implies that two variables are uncorrelated. We report also the measurement of the correlation between proton and deuteron numbers in this work.

3. Analysis methods

The results presented here are measured in minimum-bias [7] Au+Au collisions at $\sqrt{s_{\rm NN}}$ = 7.7 to 200 GeV recorded using the STAR detector at RHIC. Collision events are selected having the vertex position (V_z) within ±30 cm (±40 cm for $\sqrt{s_{\rm NN}}$ = 7.7 GeV) with respect to the nominal center of the STAR Time Projection Chamber (TPC) detector along the beam direction (z axis). Events at each collision energy are further divided into centrality classes using the produced charged particle multiplicity as a measure. Central collision events have higher values of charged particle multiplicity compared to peripheral collision events. The charged particle multiplicity used for the centrality classification is selected using the TPC detector with pseudorapidity (η) within -1 to $+1$. Protons, deuterons, and their anti-particles are removed from the definition of collision centrality. This avoids the self-correlation effect between deuterons used to calculate cumulants and particles included in the centrality definition [41–44]. The results presented here correspond to three event classes: most central collisions (events from the top 5% of the above-mentioned multiplicity distribution), mid-central (events from 30-40% of the distribution), and peripheral collisions (events from 70-80% of the distribution). The number of analyzed events at each energy is provided in Table 1. The charged tracks used for the cumulant analysis are

Table 1: Total event statistics (in millions) for Au+Au collisions at various $\sqrt{s_{\rm NN}}$.

$\sqrt{s_{NN}}$ (GeV)	7.7	11.5	14.5	19.6	27	39	54.4	62.4	200
Events	2.2	6.6	12	14	30	83	520	37	220

required to have more than 20 space points in the TPC to ensure good track momentum resolution and the ratio between assigned to total possible space points is taken to be greater than 0.52 in order to minimize track splitting. The distance of the closest approach (DCA) of the selected tracks to the primary vertex is required to be within 1 cm in order to suppress contamination from secondary particles [45, 46]. To identify deuterons and protons, particle identification (PID) selection criteria are further applied to the charged tracks. PID is done via ionization energy loss (dE/dx) measured in the TPC [47] and mass squared (m^2) obtained from the Time Of Flight (TOF) [48] detectors. Panel (a) in Fig. 1 shows the measured $\langle dE/dx\rangle$ vs. rigidity (*i.e.* momentum/charge) of particles in $|\eta| < 1.0$. Various bands corresponding to particles of different masses are clearly separated at low momentum. An extension of PID to higher $p_{\rm T}$ is achieved by using the TOF detector. Panel (b) in

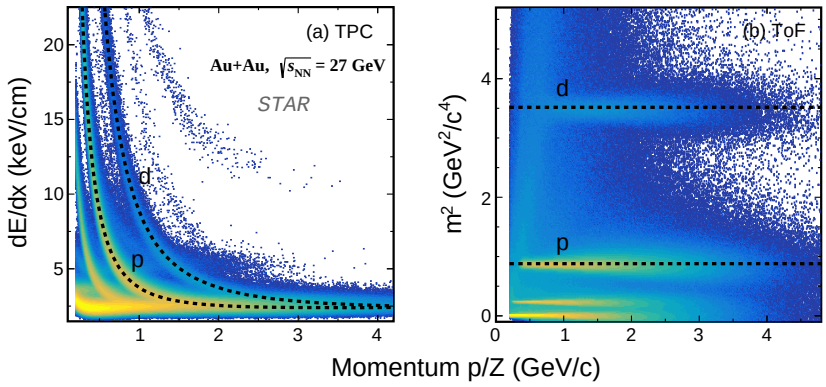

Figure 1: $\langle dE/dx \rangle$ and m^2 distribution of charged particles for $|\eta| < 1.0$ in Au+Au collisions at $\sqrt{s_{NN}}$ = 27 GeV. Panel (a): The $\langle dE/dx \rangle$ distribution of charged particles from TPC [47] as a function of rigidity (p/Z). The dashed curves represent the expected values of $\langle dE/dx \rangle$ calculated using the Bichsel function [49] for the corresponding particles. Panel (b): Mass squared of charged particles as a function of momentum from TOF [48]. The dashed lines represent the mass squared values for the corresponding particles.

Fig. 1 shows the distribution of m^2 calculated using the information (path length and time of travel by the particle) from the TOF detector. The kinematic region for deuterons covers the full azimuth range, mid-rapidity ($|y| < 0.5$), and the p_T range is from 0.8 to 4 GeV/c. Both TPC and TOF are used to get good purity, above 98%, of the deuteron sample. For proton-deuteron correlation measurement, protons are identified at mid-rapidity with p_T between 0.4 and 2.0 GeV/c. To ensure good efficiency for the proton sample, for the p_T range $0.4 < p_T < 0.8$ GeV/c, only TPC is used while both TPC and TOF detectors are simultaneously used for the range $0.8 < p_T < 2.0$ GeV/c [44]. For the momentum ranges studied, the typical value of the TPC tracking (TOF-matching) efficiency for deuterons in 0-5% most central collisions at $\sqrt{s_{NN}}$ = 7.7 GeV is 81% (69%). The corresponding values at $\sqrt{s_{NN}}$ = 200 GeV are 63% (64%). Protons are identified with similar values of detection efficiencies [44].

The cumulants are corrected for finite track reconstruction efficiency in the TPC and track matching efficiency in TOF detectors. The correction is performed assuming a binomial response of both detectors for deuteron and proton efficiencies [50]. In addition, cumulants are corrected for their dependence on multiplicity by using the Centrality Bin-Width Correction (CBWC) method [41] for each centrality. This correction suppresses the effect of initial volume fluctuations on the measured cumulants arising due to fluctuations in the impact parameter of collisions.

The statistical uncertainties on the measurements are calculated using a Monte Carlo approach called the Bootstrap method [51, 52]. The systematic uncertainties are estimated by varying the track selection and particle identification criteria. Track quality cuts such as DCA, the number of space points in the TPC, and PID criteria such as cuts on measured dE/dx and m^2 values are considered as the sources of systematic uncertainty [44]. In addition, a ±5% uncertainty associated with the reconstruction efficiency of the detector is also included in the overall systematic uncertainty. For each source of systematics, the standard deviation from the default set of results is calculated. The systematic uncertainty is determined from the square root of the quadratic sum of the standard deviations coming from different sources. The typical systematic errors, for example in 0-5% most central collisions at 7.7 GeV, are of the order of 5% for C_1, C_2, and C_3 and 6% for C_4. The uncertainty in the reconstruction efficiency estimation makes the biggest contribution to the systematics.

4. Results and discussion

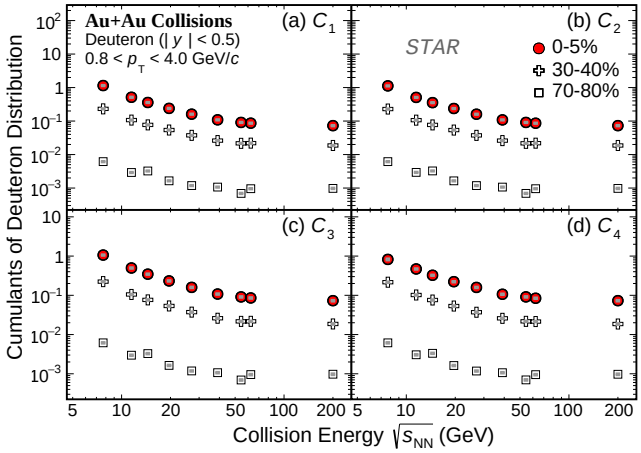

Figure 2: Cumulants (C_n, $n = 1 - 4$) of the deuteron distributions as a function of collision energy for most central (0-5%) mid-central (30-40%) and peripheral (70-80%) Au+Au collisions as measured by STAR. Cumulants are corrected for finite detector efficiencies [50] and centrality bin-width effect [41]. Uncertainties on the cumulants are smaller than marker symbols. Results for most central, mid-central, and peripheral collisions are shown using solid circle, open cross, and open square markers, respectively. Bar and cap symbols represent the statistical and systematic uncertainties, respectively. The transverse momentum (p_T) range for the measurements is from 0.8 to 4 GeV/c and the rapidity (y) range is $-0.5 < y < 0.5$.

Figure 2 shows the deuteron cumulants (C_n, $n = 1 - 4$) as a function of $\sqrt{s_{NN}}$ for most central (0-5%), mid-central (30-40%), and peripheral (70-80%) Au+Au collisions. The cumulants C_1 to C_4 of deuteron distributions for most central Au+Au

collisions smoothly increase with decreasing $\sqrt{s_{\rm NN}}$. This indicates an enhanced production of deuterons towards the high baryon density region (corresponding to low $\sqrt{s_{\rm NN}}$ [7]). The effect of high baryon density on deuteron production can be understood using a thermal model. In the thermal model, baryon density dependence is given by the factor $\sim \exp[(B\mu_B - m_d)/T]$, where B and m_d are the baryon number and mass of the deuteron, respectively. As light nuclei carry multiple baryons, the contribution of the above factor is especially enhanced in the high baryon density region. Cumulants in the mid-central and peripheral collisions show a similar $\sqrt{s_{\rm NN}}$ dependence as seen for the most central collisions. For any given $\sqrt{s_{\rm NN}}$, the cumulants of any order increase from peripheral to central collisions. For $\sqrt{s_{\rm NN}}$ = 27 GeV and above, in any given collision energy and centrality, C_1 to C_4 values are close to each other and almost independent of order (n) of the cumulant. This implies that the event-by-event deuteron number distribution at higher $\sqrt{s_{\rm NN}}$ exhibit a near-Poissonian behavior. Figure 3 shows the collision energy dependence of the cumulant ratios and the proton-deuteron number Pearson correlation coefficient for most central 0-5% and peripheral 70-80% Au+Au collisions. The cumulant ratios $\kappa\sigma^2$, $S\sigma$, and σ^2/M in central collisions show smooth dependence on collision energy. At higher colliding energies ($\sqrt{s_{\rm NN}} \geq 27$ GeV), most central 0-5% cumulant ratios are close to the Poisson baseline (unity) and deviate from unity as $\sqrt{s_{\rm NN}}$ decreases. In low-energy collisions, cumulants are increasingly suppressed with increasing order n, resulting in the $\kappa\sigma^2$ showing the largest deviation from unity compared to the other two ratios which involve lower-order cumulants. Note that the scales of the y-axis are different in different panels. The observed suppression of cumulant ratios might arise because of global baryon number conservation, which can notably affect the measurements performed at mid-rapidity in low-energy collisions. In low-energy collisions ($\sqrt{s_{\rm NN}} < 27$ GeV), due to an increase in the number of net baryons at mid-rapidity [53] and the acceptance cuts which include a larger fraction of the phase space, one observes an enhanced effect of baryon number conservation. Corresponding results in 70-80% peripheral centrality show a weak dependence on collision energy and are close to unity. Cumulant ratios for peripheral collisions are found to be least affected by the global baryon number conservation. Cumulant ratio values in 30-40% centrality lie between those for most central and peripheral collisions [1].

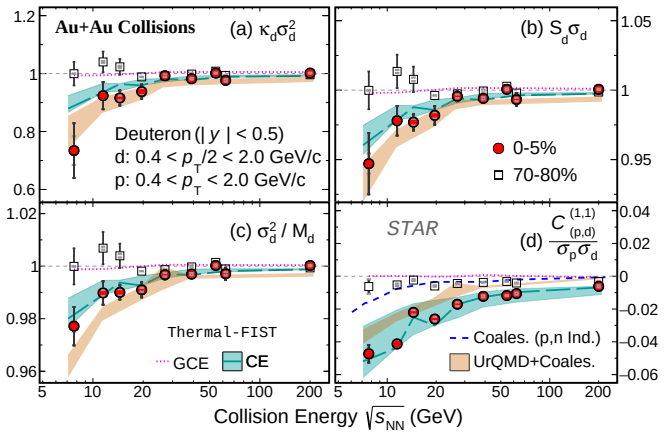

Figure 3: Cumulant ratios of deuteron distributions and proton-deuteron correlation shown as a function of collision energy. Red circle and open square markers represent measurements for most central (0-5%) and peripheral (70-80%) collisions, respectively. Bar and cap symbols represent the statistical and systematic uncertainties, respectively. The gray dashed line is the Poisson baseline (unity for cumulant ratios and zero for correlation). All model results presented in the figure correspond to the most central (0-5%) collisions. Calculations from an UrQMD coupled with a phase-space coalescence model [39] are shown using the orange color-filled band (the width of the band represents the statistical uncertainty). Thermal-FIST [36] calculations for GCE are shown using a magenta dashed line. The cyan color-filled band represents the CE thermal model results corresponding to the range of canonical correlation volume (V_c) from $2dV/dy$ to $4dV/dy$. CE thermal model results for χ^2 minimum fit of the above-mentioned four observables is shown using a cyan color dashed line. In panel (d), results for one of the assumptions in the simplified model of the coalescence process from Ref. [29] are shown using a blue dashed line.

The results from the Thermal-FIST [36] model for the most central 0-5% collisions are also shown in Fig. 3. This model assumes an ideal gas of hadrons and resonances in thermodynamic equilibrium. Model calculations are presented for both grand canonical and canonical ensembles and the experimental acceptances have been taken into account. The freeze-out parameters which are input to the model are taken from the thermal model fits of hadronic yields and spectra measured in the STAR experiment [7]. Results for the cumulant ratios from the GCE framework of the Thermal-FIST model are close to unity across all collision energies. At higher collision energies, the cumulant ratios in most central 0-5% show reasonable agreement with both GCE and CE thermal model expectations. However, GCE seems to fail to describe the ratios for $\sqrt{s_{\rm NN}} \leq 20$ GeV. The CE thermal model which incorporates baryon number conservation, predicts the suppression of cumulant ratios as observed in the data. The canonical ensemble in the Thermal-FIST model uses an additional volume parameter called the canonical correlation volume, V_c, over which the exact conservation of the baryon number is implemented. The shaded band represents the results for V_c in the range of 2 to 4 times the dV/dy, where dV/dy is the chemical freeze-out volume per unit rapidity that is obtained from the thermal model fit of hadronic yields [7]. The model parameter V_c is also varied at each collision energy for a reasonable agreement with the measured values of $\kappa\sigma^2$, $S\sigma$, σ^2/M, and the Pearson coefficient. The line shows the results corresponding to minimum χ^2 fits by scanning the V_c parameter in the model. V_c values are found to vary from $2dV/dy$ at the lowest energy to $4dV/dy$ at the highest RHIC collision energy. A slightly higher range of V_c is obtained at LHC energies for measurements from the ALICE collaboration [54, 55]. The higher value of canonical correlation volume implies that the part of the system under measurement is approaching the grand-canonical limit [54]. This also highlights the importance of the canonical ensemble thermal model at lower collision energies.

Results on cumulant ratios for 0-5% Au+Au collisions from

[1] Data points for 30-40% centrality are not presented in Fig. 3 to avoid clutter. However, the relevant results can be found in the HEPData database.

the UrQMD model combined with the phase-space coalescence mechanism are compared to the experimental data. Phase space information of protons and neutrons at the kinetic freeze-out surface from the UrQMD model are used as inputs to the coalescence mechanism [39] to form deuterons. These model results which incorporate the law of baryon number conservation combined with the coalescence mechanism, also reproduce the energy dependence trend observed in data and show a fair agreement with the measured cumulant ratios.

In panel (d) of Fig. 3, we observe that the Pearson correlation coefficient between proton and deuteron numbers is negative across all collision energies and centralities presented, which implies that the proton and deuteron numbers are anti-correlated with each other. At lower colliding energy, anti-correlation becomes stronger for most central 0-5% Au+Au collisions. These measurements for peripheral Au+Au collisions do not show any energy dependence and are close to the statistical expectations. The GCE thermal model fails to predict the observed anti-correlation between proton and deuteron. However, the CE thermal model calculation correctly predicts the sign and energy dependence trend of the correlation. Predictions from the simple statistical simulation of the coalescence process from Ref. [29] are shown also for most central Au+Au collisions. Two different assumptions about the proton and neutron number are utilized in this model, namely, in one case, they are fully correlated (*i.e.* $N_p = N_n$, where N_p and N_n are the proton and neutron multiplicities, respectively) and in the other case, they are independent. Neither correlated nor independent assumptions for proton and neutron numbers in the model reproduce the data for most central collisions. The fully correlated assumption in the model fails to predict the sign of the correlation and we do not present those results here. Note that this model does not take into account the details of the phase space information of coalescing protons and neutrons. On the other hand, the fair agreement of predictions from the UrQMD model combined with the phase-space coalescence mechanism [39] with the experimental data in most central 0-5% collisions suggests that the phase-space information of constituent nucleons is important for the deuteron formation process in the coalescence mechanism. The ALICE collaboration recently reported measurements on proton-deuteron correlation for Pb+Pb collisions at $\sqrt{s_{\rm NN}}$ = 5.02 TeV. The Pearson correlation coefficient was found to have small negative values and is mostly constant for all collision centralities [56]. Similar to the observations of this study, the CE thermal model calculations with baryon number conservation implemented also explain the ALICE data for suitable choices of model parameters. The negative sign of the Pearson correlation coefficient across the range of collision energies (GeV to TeV) and centralities (central to peripheral) establishes the importance of baryon number conservation in baryon-nucleus correlations. The nature of the agreement of the proton-deuteron correlation data with the CE thermal model calculation suggests a canonical thermal effect over a coalescence mechanism. At the same time, there is reasonable scope for improvements in both the production models discussed here.

As deuterons carry two baryons, it is important and interesting to investigate how their cumulant ratios differ from those

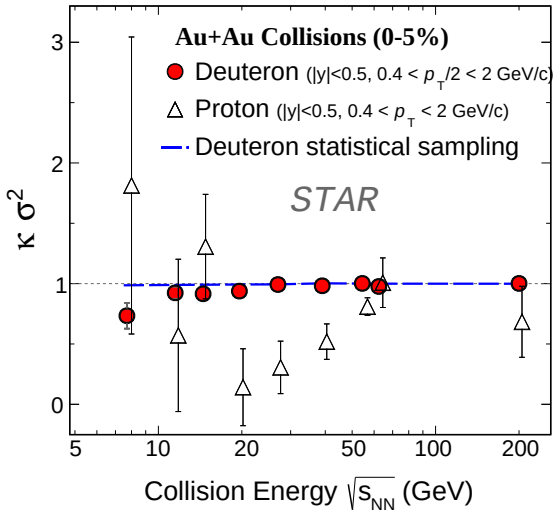

Figure 4: $\kappa\sigma^2$ of deuteron and proton distribution for most central (0-5%) Au+Au collisions. Red circle and black triangle markers represent deuteron and proton data [44], respectively. The gray dashed line is the Poisson baseline (unity). $\kappa\sigma^2$ of deuterons show a smooth dependence on the collision energy in contrast to protons.

of the protons. We have compared deuteron cumulant ratios to those already published measurements for protons. Figure 4 shows the comparison of $\kappa\sigma^2$ of the deuteron multiplicity distribution to those of protons [44] for most central 0-5% Au+Au collisions. For the $\kappa\sigma^2$ of protons, the larger statistical uncertainties are attributed to the larger width of proton multiplicity distributions as compared to the deuteron distributions [51]. Within the current uncertainties, the proton $\kappa\sigma^2$ (similar to that of net-proton) shows a non-monotonic $\sqrt{s_{\rm NN}}$ dependence [43] in most central Au+Au collisions. This feature is similar, at a qualitative level, to the theoretical predictions near the QCD critical point. The $\kappa\sigma^2$ for deuterons, however, shows a weaker dependence on collision energy compared to that for protons. This could be due to deuterons having a very low event-by-event yield compared to protons, resulting in reduced sensitivity to any possible critical point physics. To test the effect of low event-by-event yield on the cumulant ratios, a simple statistical simulation is utilized by using the measured deuteron to proton yield ratios [10] and proton cumulants [44] as inputs. Using a two-component function, which is a superposition of Poisson and binomial distributions (originally developed in Ref. [57] for a different purpose), the proton distribution is modeled in order to reproduce the measured proton cumulants in most central 0-5% Au+Au collisions. Then deuteron multiplicity on an event-by-event basis is sampled from the above-mentioned proton distribution using the d/p ratio [10] as the binomial probability of success to form a deuteron. The $\kappa\sigma^2$ calculated from this resultant deuteron distribution (shown in Fig. 4 as a blue dashed line) is near unity and close to the experimental data. This test shows that the low deuteron multiplicity likely is responsible for the deuteron $\kappa\sigma^2$ being close to 1.

5. Summary

We have presented measurements of deuteron cumulants, their ratios, and proton-deuteron number correlation performed in Au+Au collisions with the STAR detector at RHIC, covering a wide range of baryon chemical potential (μ_B from $\sim$ 20 to 420 MeV). The cumulant ratios of deuterons in most central collisions vary smoothly as a function of the collision energy and are suppressed below the Poisson baseline as the colliding energy decreases. The peripheral collision results, however, remain overall flat as a function of $\sqrt{s_{\rm NN}}$. Anti-correlation between proton and deuteron numbers is observed across all collision energies and centralities studied. This anti-correlation becomes stronger for most central Au+Au collisions as the beam energy decreases. Cumulant ratios and correlations in mid-central collisions show a weaker dependence on collision energies compared to central collisions. These measurements for peripheral Au+Au collisions do not show a significant energy dependence and are close to statistical expectations.

Important observations from the comparison of our measurements to the different model calculations can be summarized as follows. In most central Au+Au collisions, for thermal models: (i) GCE and CE reasonably describe the deuteron number fluctuation measurements above collision energies of 20 GeV. Only the CE model correctly predicts the negative sign of the proton-deuteron correlation. (ii) The thermal model with CE qualitatively agrees with the cumulant ratios for collision energies below 20 GeV, while the thermal model with GCE fails. As the CE model explicitly conserves the baryon number, this study reflects the importance of the role of conservation in fluctuation studies at lower collision energies.

The UrQMD model coupled with a phase-space coalescence mechanism also describes the deuteron number fluctuation and deuteron-proton correlation measurements across all collision energies. A simplified modeling of the coalescence process without taking into account the phase-space information of constituent nucleons fails to describe the measured proton-deuteron number correlation.

The $\kappa\sigma^2$ of the deuteron number distribution shows a smoothly decreasing trend with decreasing collision energy in contrast to protons. A simple statistical test suggests that the low deuteron multiplicity may be responsible for the observed near-Poisson behavior of deuteron cumulant ratios. Our measurements can be utilized further to study the chemical freeze-out thermodynamics of deuterons and to constrain the light nuclei production model parameters. In the future, with higher event statistics and improved acceptance, $p_{\rm T}$ and rapidity differential measurements of light nuclei fluctuations and hadron-nuclei correlations with better statistical and systematic precision are possible. This has the potential for a major improvement in the discriminating power of comparisons with model calculations and might help resolve the nuclei production puzzle in high-energy heavy-ion collisions.

Acknowledgements: We thank the RHIC Operations Group and RCF at BNL, the NERSC Center at LBNL, and the Open Science Grid consortium for providing resources and support. This work was supported in part by the Office of Nuclear Physics within the U.S. DOE Office of Science, the U.S. National Science Foundation, National Natural Science Foundation of China, Chinese Academy of Science, the Ministry of Science and Technology of China and the Chinese Ministry of Education, the Higher Education Sprout Project by Ministry of Education at NCKU, the National Research Foundation of Korea, Czech Science Foundation and Ministry of Education, Youth and Sports of the Czech Republic, Hungarian National Research, Development and Innovation Office, New National Excellency Programme of the Hungarian Ministry of Human Capacities, Department of Atomic Energy and Department of Science and Technology of the Government of India, the National Science Centre and WUT ID-UB of Poland, the Ministry of Science, Education and Sports of the Republic of Croatia, German Bundesministerium für Bildung, Wissenschaft, Forschung and Technologie (BMBF), Helmholtz Association, Ministry of Education, Culture, Sports, Science, and Technology (MEXT) and Japan Society for the Promotion of Science (JSPS).

References

[1] I. Arsene et al., BRAHMS Collaboration, Nucl. Phys. A 757 (2005) 1–27.
[2] B. B. Back et al., PHOBOS Collaboration, Nucl. Phys. A 757 (2005) 28–101.
[3] J. Adams et al., STAR Collaboration, Nucl. Phys. A 757 (2005) 102–183.
[4] K. Adcox et al., PHENIX Collaboration, Nucl. Phys. A 757 (2005) 184–283.
[5] S. Chatrchyan et al., CMS Collaboration, JHEP 05 (2012) 063.
[6] [ALICE Collaboration], [arXiv:2211.04384 [nucl-ex]].
[7] L. Adamczyk et al., STAR Collaboration, Phys. Rev. C 96 (2017) 044904.
[8] J. Adams et al., STAR Collaboration, Phys. Rev. Lett. 92 (2004) 112301.
[9] A. Andronic, P. Braun-Munzinger, K. Redlich and J. Stachel, Nature 561 (2018) 321–330.
[10] J. Adam et al., STAR Collaboration, Phys. Rev. C 99 (2019) 064905.
[11] J. Adam et al., ALICE Collaboration, Phys. Rev. C 93 (2016) 024917.
[12] T. Anticic et al., NA49 Collaboration, Phys. Rev. C 94 (2016) 044906.
[13] S. Chatterjee and B. Mohanty, Phys. Rev. C 90 (2014) 034908.
[14] D. Biswas, Phys. Rev. C 102 (2020) 054902.
[15] S. T. Butler and C. A. Pearson, Phys. Rev. 129 (1963) 836–842.
[16] J. I. Kapusta, Phys. Rev. C 21 (1980) 1301–1310.
[17] T. Z. Yan, Y. G. Ma, X. Z. Cai, J. G. Chen, D. Q. Fang, W. Guo, C. W. Ma, E. J. Ma, W. Q. Shen and W. D. Tian, et. al., Phys. Lett. B 638 (2006) 50–54.
[18] L. Adamczyk et al., STAR Collaboration, Phys. Rev. C 94 (2016) 034908.
[19] S. Mrowczynski, J. Phys. G 13 (1987) 1089–1097.
[20] R. Scheibl and U. W. Heinz, Phys. Rev. C 59 (1999) 1585–1602.
[21] A. Andronic, P. Braun-Munzinger, J. Stachel and H. Stocker, Phys. Lett. B 697 (2011) 203–207.
[22] S. Mrowczynski, Acta Phys. Polon. B 48 (2017) 707.
[23] M. A. Stephanov, K. Rajagopal and E. V. Shuryak, Phys. Rev. D 60 (1999) 114028.
[24] F. Karsch and K. Redlich, Phys. Lett. B 695 (2011) 136–142.
[25] S. Borsanyi, Z. Fodor, S. D. Katz, S. Krieg, C. Ratti and K. K. Szabo, Phys. Rev. Lett. 113 (2014) 052301.
[26] P. Alba, W. Alberico, R. Bellwied, M. Bluhm, V. Mantovani Sarti, M. Nahrgang and C. Ratti, Phys. Lett. B 738 (2014) 305–310.
[27] S. Gupta, D. Mallick, D. K. Mishra, B. Mohanty and N. Xu, Phys. Lett. B 829 (2022) 137021.
[28] A. Pandav, D. Mallick and B. Mohanty, Prog. Part. Nucl. Phys. 125 (2022) 103960.
[29] Z. Fecková, J. Steinheimer, B. Tomášik and M. Bleicher, Phys. Rev. C 93 (2016) 054906.
[30] E. Shuryak and J. M. Torres-Rincon, Phys. Rev. C 100 (2019) 024903.

[31] E. Shuryak and J. M. Torres-Rincon, Phys. Rev. C 101 (2020) 034914.
[32] K. J. Sun, L. W. Chen, C. M. Ko and Z. Xu, Phys. Lett. B 774 (2017) 103–107.
[33] [STAR Collaboration], [arXiv:2209.08058 [nucl-ex]].
[34] K. H. Ackermann et al., STAR Collaboration, Nucl. Instrum. Meth. A 499 (2003) 624–632.
[35] J. Cleymans, H. Oeschler, K. Redlich and S. Wheaton, Phys. Rev. C 73 (2006) 034905.
[36] V. Vovchenko and H. Stoecker, Comput. Phys. Commun. 244 (2019) 295–310.
[37] M. Bleicher, E. Zabrodin, C. Spieles, S. A. Bass, C. Ernst, S. Soff, L. Bravina, M. Belkacem, H. Weber and H. Stoecker, et. al., J. Phys. G 25 (1999) 1859–1896.
[38] H. Petersen, M. Bleicher, S. A. Bass and H. Stocker, [arXiv:0805.0567 [hep-ph]].
[39] S. Sombun, K. Tomuang, A. Limphirat, P. Hillmann, C. Herold, J. Steinheimer, Y. Yan and M. Bleicher, Phys. Rev. C 99 (2019) 014901.
[40] S. Gupta, PoS CPOD2009 (2009) 025.
[41] X. Luo, J. Xu, B. Mohanty and N. Xu, J. Phys. G 40 (2013) 105104.
[42] A. Chatterjee, Y. Zhang, J. Zeng, N. R. Sahoo and X. Luo, Phys. Rev. C 101 (2020) 034902.
[43] J. Adam et al., STAR Collaboration, Phys. Rev. Lett. 126 (2021) 092301.
[44] M. Abdallah et al., STAR Collaboration, Phys. Rev. C 104 (2021) 024902.
[45] B. I. Abelev et al., STAR Collaboration, Phys. Lett. B 655 (2007) 104–113.
[46] B. I. Abelev et al., STAR Collaboration, Phys. Rev. C 79 (2009) 034909.
[47] M. Anderson, J. Berkovitz, W. Betts, R. Bossingham, F. Bieser, R. Brown, M. Burks, M. Calderon de la Barca Sanchez, D. A. Cebra and M. G. Cherney, et. al., Nucl. Instrum. Meth. A 499 (2003) 659–678.
[48] W. J. Llope, Nucl. Instrum. Meth. B 241 (2005) 306–310.
[49] H. Bichsel, Nucl. Instrum. Meth. A 562 (2006) 154–197.
[50] T. Nonaka, M. Kitazawa and S. Esumi, Phys. Rev. C 95 (2017) 064912.
[51] X. Luo, Phys. Rev. C 91 (2015) 034907.
[52] A. Pandav, D. Mallick and B. Mohanty, Nucl. Phys. A 991 (2019) 121608.
[53] F. Videbaek and O. Hansen, Phys. Rev. C 52 (1995) 2684–2693.
[54] V. Vovchenko, B. Dönigus and H. Stoecker, Phys. Rev. C 100 (2019) 054906.
[55] V. Vovchenko and V. Koch, Phys. Rev. C 103 (2021) 044903.
[56] [ALICE Collaboration], [arXiv:2204.10166 [nucl-ex]].
[57] A. Bzdak, V. Koch, D. Oliinychenko and J. Steinheimer, Phys. Rev. C 98 (2018) 054901.